

See discussions, stats, and author profiles for this publication at: <https://www.researchgate.net/publication/370249873>

# Numerical Approach to Simulation of Geometry Variation during Sintering of Ceramics Based on the Finite Element Method

Article in *Journal of Applied and Industrial Mathematics* · May 2023

DOI: 10.1134/S1990478923010209

CITATIONS

0

READS

44

7 authors, including:



**Olga A Solnyshkina**

Ufa university of science and technology

41 PUBLICATIONS 63 CITATIONS

[SEE PROFILE](#)



**Nazgul B. Fatkullina**

Bashkir State University

7 PUBLICATIONS 3 CITATIONS

[SEE PROFILE](#)



**Aiguzel Z. Bulatova**

Bashkir State University

6 PUBLICATIONS 3 CITATIONS

[SEE PROFILE](#)



**Victor Nicolaevich Kireev**

Bashkir State University

45 PUBLICATIONS 47 CITATIONS

[SEE PROFILE](#)

Some of the authors of this publication are also working on these related projects:



Bladder cancer [View project](#)



Personalized ceramic medical implants [View project](#)

# Numerical Approach to Simulation of Geometry Variation during Sintering of Ceramics Based on the Finite Element Method

O. A. Solnyshkina<sup>1,2\*</sup>, N. B. Fatkullina<sup>1,2\*\*</sup>, A. Z. Bulatova<sup>1,2\*\*\*</sup>,  
V. N. Kireev<sup>1,2\*\*\*\*</sup>, A. R. Bilyalov<sup>1\*\*\*\*\*</sup>, I. S. Akhatov<sup>1\*\*\*\*\*</sup>,  
and V. N. Pavlov<sup>1\*\*\*\*\*</sup>

<sup>1</sup>*Bashkir State Medical University, Ufa, 450008 Russia*

<sup>2</sup>*Center for Micro- and Nanoscale Dynamics of Dispersed Systems, Ufa University of Science and Technology, Ufa, 450076 Russia*

*e-mail: \*olgasolnyshkina@gmail.com, \*\*nazgulbay@mail.ru, \*\*\*bulatova29@yandex.ru, \*\*\*\*kireev@anrb.ru, \*\*\*\*\*azat.bilyalov@gmail.com, \*\*\*\*\*iskander.akhatov@gmail.com, \*\*\*\*\*rectorat@bashgmu.ru*

Received August 4, 2022; revised August 4, 2022; accepted September 29, 2022

**Abstract**—Sintering is a complex physical and mechanical process, which is one of the most important technological processes in powder metallurgy and ceramic industry. In this paper, the study of free sintering of a ceramic object is carried out using the rheological theory of sintering. Numerical solution of the problem in the three-dimensional case is implemented using the Finite Element Method with the freely distributed FreeFem++ software. Experiments on sintering of aluminium oxide ceramic paste were conducted for several temperature regimes. The validation of the realized model is confirmed by comparing the numerical and experimental data of porosity evolution.

**Keywords:** *rheological sintering model, 3D printing, ceramic powder, aluminium oxide, numerical simulation, finite element method*

**DOI:** 10.1134/S1990478923010209

## INTRODUCTION

Additive manufacturing technologies and approaches of are widely used in various fields of science and industry, especially in cases where of critical importance is the manufacture of complex structures or small-scale or individual production [1]. In recent years, 3D printing technologies have been used in the manufacture of ceramic implants in medicine [2], since they have good biocompatibility. The process of manufacturing ceramic implants using 3D printing technology can be divided into several stages, viz., designing a three-dimensional computer model in CAD systems, printing the product as such, and the final processing stage, which includes multistage sintering under various conditions. The basic principle of the sintering process is the consolidation of loose or loosely bound powders at elevated temperatures close to the melting point with and without applying external (electromagnetic, pressure) fields.

The sintering process is usually described in three stages [3] (see Fig. 1). At an early or initial stage, so-called necks are formed between individual particles (the zone of intergranular contact indicated in Fig. 1), and compaction is regulated by neck growth [4]. Particles can slide and rotate, forming lower energy interfaces that promote grain growth. As the neck width increases and particle coalescence increases, the pore sizes decrease. Migration of material to free surfaces and back stops. Densification is largely limited by grain boundaries and diffusion. This limited-diffusion phase is characteristic of the intermediate sintering stage, in which the pores remain interconnected. At the final stage of sintering, the channels between the grains are closed, and isolated pores are formed. Kinetic phenomena at the final stage are usually modeled as phenomena in bulk material. At all

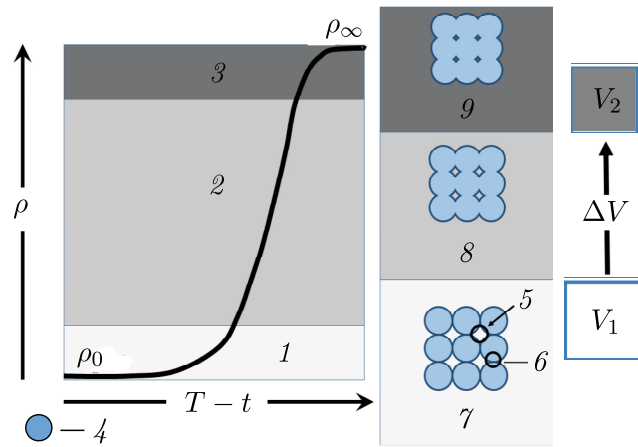


**Fig. 1.** Ceramic powder sintering stages: initial stage (1), intermediate stage (2), final stage (3), ceramic powder particles (4), pore (5), “neck” (6), “neck” zone formation (7), isolated pores (8), and bound pores (9).

three stages, the material is compacted and, as a result, a substantial change in the volume and shape of the sample occurs, with its porosity decreasing on average by 30–35%. In this regard, the task of more accurate prediction of the shape of the final ceramic product is especially relevant.

Depending on the scale of the medium under consideration, approaches to modeling sintering can be divided into atomic, microstructural, and continuum ones. The main tool for obtaining the fundamental characteristics of the process at the nano- and microlevels is the methods of molecular dynamics [5, 6]. Molecular dynamic modeling has been successfully used to study the mechanisms of sintering and the evolution of the microstructure of nanosized powders [7] and to calculate the diffusion coefficient of metals and the diffusion of ions in ceramics. However, modeling at the particle level, and even more so the prediction of the shape of the final product at the macroscopic level, is most often carried out using micromechanical and continuum approaches. The discrete element methods [8], Monte Carlo kinetic methods [9], the phase field method [10], and the boundary element method [1] are used to simulate the kinetics of grain growth and changes in the sample microstructure.

In most models, sintering was considered as a collective result of thermally activated adhesion processes leading to an increase in contacts between particles and their coalescence. The developed approaches were mainly aimed at studying the mechanisms of interparticle interaction, i.e., at studying the local kinetics of the process. However, the sintering kinetics of real porous bodies is determined not only by the properties of powder particles and the nature of their interaction, but also by macroscopic factors. These include kinematic limitations (for example, adhesion of the end of a porous sample to the furnace surface), applied external forces, as well as inhomogeneity of properties in the volume under study. These problems can be solved only within the framework of a macroscopic description, which should be based on concepts that are fundamentally different from the representations of local analysis.

A promising approach to solving this problem is associated with the use of ideologies from continuum mechanics, which are successfully used to describe the compaction of porous bodies and are based on theories of plastic deformation of porous bodies. One of the most characteristic outward manifestations of the process of sintering a porous body is a change (decrease) in its linear dimensions. This makes it possible to consider sintering as some macroscopic process of deformation of the volume and shape of a porous body carried out by the flow of matter in the solid phase. Since the internal structure of the porous space is inhomogeneous, the velocities of the flow of matter in microvolumes are also inhomogeneous, with the local values being random quantities. At the same time, the field of macroscopically averaged flow velocities can be close to homogeneous in many cases, for example, during sintering of porous bodies with a uniform macroscopic density. In this sense, sintering can be considered as a subject of rheological study [12]. The optimization of sintering processes for real parts is currently only possible using a macroscopic approach based on continuum

mechanics. In addition, the continuum theory of sintering allows generalizations, including the impact of various fields [4, 13].

One of the key tasks in the development of the ceramic 3D printing industry is the selection of the correct model for predicting the behavior of a particular material during the manufacturing process. The purpose of this work is to develop a mathematical approach to three-dimensional modeling of changes in the volume and shape of a ceramic product during sintering. Since the properties and parameters of each particular ceramic powder significantly affect the kinetics of the sintering process and, as a result, the change in the macroscopic parameters of the product, the model was validated using experimental data.

## 1. MATHEMATICAL STATEMENT OF THE PROBLEM

Representations of macrorheology are used in formulating the law of behavior of a porous body under the action of external forces, as well as taking into account the action of driving forces of sintering. The driving forces of sintering in the rheological theory of sintering are related to the action of the Laplace pressure (sintering potential or sintering stress). It is assumed that external interactions and driving forces make an additive contribution to the behavior of a porous body and that changes in shape and volume are irreversible.

Let us describe in more detail the main equations of this approach. The continuum theory determines the behavior of a compressible continuous medium during sintering, by analogy with the theory of elasticity, by the following equation relating the stress tensor  $\sigma_{ij}$  and the strain rate tensor  $\varepsilon_{ij}$ , which in the Cartesian coordinate system has the form [14, 15]

$$\sigma_{ij} = \frac{\sigma(W)}{W} \left[ \varphi \varepsilon_{ij} + \left( \psi - \frac{1}{3} \varphi \right) \dot{\varepsilon} \delta_{ij} \right] + P_L \delta_{ij}, \quad i, j = 1, 2, 3, \quad (1)$$

where  $W$  and  $\sigma(W)$  are the equivalent strain rate and stress that correspond to the behavior of the dense phase,  $\varphi$  and  $\psi$  are the shear and bulk modulus of viscosity,  $\delta_{ij}$  is the Kronecker symbol, and  $\dot{\varepsilon}$  is the first invariant of the strain rate tensor, i.e., the sum  $\dot{\varepsilon} = \varepsilon_{11} + \varepsilon_{22} + \varepsilon_{33}$  of the diagonal components (for the 3D case). Physically,  $\dot{\varepsilon}$  reflects the change in the volume of the porous body.

The effective equivalent of the strain rates depends on the invariants of the strain rate tensor as follows:  $W = \frac{1}{\sqrt{1-\theta}} \sqrt{\varphi \dot{\gamma}^2 + \psi \dot{\varepsilon}^2}$ , where  $\dot{\gamma}$  is the second invariant of the strain rate tensor, the physical meaning of which is the rate of change in the shape of the porous body.

In this paper, we consider a model for describing the change in the porosity of ceramic products during manufacture using 3D printing by laser stereolithography (SLA). In this case, in terms of technology, the sintering process occurs without applying external fields or external pressure—the so-called free sintering. During unpressurized sintering, low stresses occur and it is assumed that diffusion or viscous mechanisms are the dominant transport mechanisms. These mechanisms are linear, with the following linear relation satisfied [3]:

$$\sigma(W) = 2\eta W, \quad (2)$$

where  $\eta$  is the shear viscosity of the material. Then, taking into account (2), Eq. (1) can be rewritten as

$$\sigma_{ij} = 2\eta \left[ \varphi \varepsilon_{ij} + \left( \psi - \frac{1}{3} \varphi \right) \dot{\varepsilon} \delta_{ij} \right] + P_L \delta_{ij}. \quad (3)$$

The right-hand side of this equation contains the term  $P_L$ , which expresses the effective sintering stress arising due to capillary forces and is calculated using the theoretical formula presented in [12],

$$P_L = \frac{3\gamma}{r} (1 - \theta)^2, \quad (4)$$

where  $\gamma$  is the surface energy coefficient and  $r$  is the average radius of ceramic powder particles. In some modifications, a term can also be added to  $P_L$  that takes into account the gas pressure in the pores [16] or the influence of external fields.

In the simplest case, the three main parameters  $P_L$ ,  $\varphi$ , and  $\psi$  in relation (3) are functions of the porosity  $\theta$  and, in accordance with the rheological model [12, 14], can be calculated using the formulas

$$\begin{aligned} \varphi &= (1 - \theta)^2, \\ \psi &= \frac{2(1 - \theta)^3}{3\theta}. \end{aligned} \tag{5}$$

In addition, within the framework of the model, to take into account the change in the viscosity of the material with a change in temperature, an Arrhenius-type relation is used [17, 18],

$$\eta(T) = AT^n \exp(B/T), \tag{6}$$

where  $A$ ,  $B$ , and  $n$  are material constants that can be chosen by optimizing the model using experimental data for each particular material.

To calculate the change in porosity (relative density) over time, the following mass conservation equation is used:

$$\frac{\dot{\theta}}{1 - \theta} = \dot{\varepsilon} = \varepsilon_{11} + \varepsilon_{22} + \varepsilon_{33}. \tag{7}$$

In the framework of this paper, Eqs. (3)–(7) are solved using the finite element method in the case of free sintering without the application of external forces with the following boundary and initial conditions on the surface  $S$  of the simulated parallelepiped  $S$ :  $\sigma \cdot \mathbf{n} = 0$ ;  $S_1$ :  $\mathbf{u} = 0$ ;  $t = 0$ :  $\mathbf{u} = 0$ , where  $S_1$  is the bottom face of the parallelepiped. Expression (3) is an open structure of the model of the sintering process at the macrolevel that makes it possible to expand the basic model of sintering to various more complex cases [15], including due to various approaches for taking into account anisotropy.

One of the main practically significant directions in the development of continuum sintering models is the correct consideration of anisotropy when the product shape changes. Anisotropy during sintering has been observed in some experimental works [19], and the authors attribute shrinkage to the spatial distribution of elongated grains or pores during the initial stages of processing. A number of papers have proposed various approaches to solving this problem. In [20], a micromechanical model is presented that describes the evolution of the microstructure during sintering of a powder compact consisting of uniformly packed, oriented, elongated particles with elliptical pores. The authors derived constitutive equations describing shrinkage using the sintering stress tensor and the material viscosity tensor, taking into account changes in the shape of pores due to diffusion along grain boundaries in the two-dimensional case. Nevertheless, when modeling changes in the shape of real objects, it is rather problematic to take into account the microstructure of samples in which pores and grains are far from model approximations in shape.

Another ideology for taking into account anisotropy during sintering is presented in [16]. In the case of a linear sintering equation, the anisotropy can be introduced into the relation for the viscosity of the material. For the three-dimensional axisymmetric case in a cylindrical coordinate system, the formulas have the form

$$\begin{aligned} 2\eta(T)_r &= \eta_{0r}T \exp(Q/RT), \\ 2\eta(T)_z &= \eta_{0z}T \exp(Q/RT), \end{aligned} \tag{8}$$

where  $Q = 300.3$  kJ/mol is the process activation energy,  $R = 8.314$  J/(mol×K) is the universal gas constant,  $\eta_{0z} = 3 \times 10^{-3}$  Pa×s is the shear viscosity of completely dense material in various directions, and  $\eta_{0r}$  is determined from the relations described below. The necessary parameters for model tuning can be found from the experimental data of dilatometric tests of samples of specific materials.

One of the approaches takes into account the gas pressure in closed pores at the final stage [16]. On the right-hand side in Eq. (3),  $P_L$  is replaced by  $P_L - P_S$  to take into account the intrapore gas pressure  $P_S$ ,

$$\frac{P_S}{\gamma} = \frac{\eta_0}{\gamma} \exp(Q/RT) \frac{T\psi\dot{\theta}}{(1 - \theta)} + \frac{3(1 - \theta)^2}{r}.$$

**Table 1.** Experimental results

	1100 °C	1200 °C	1300 °C	1400 °C	1500 °C	1600 °C	1700 °C
$\theta_{\text{exp}}, \%$	44.91417	44.05613	44.55397	43.35036	40.22472	28.68234	5.4884
$s, \%$	0.4027	0.1658	0.2739	0.1616	0.7341	0.8808	0.9323

The model for accounting for gas pressure is supplemented by the relation for shear viscosity

$$\eta_{0r} = \eta_{0z} + 0.001\theta^{2.5}.$$

Another approach to modeling is to use a threshold law to explain the slowdown in sintering at the final stage when the critical value of porosity  $\theta_c = 0.068$  is reached instead of taking into account the pressure of gas trapped in pores,

$$\eta_{0r} = \eta_{0z} + 0.0021(\theta - \theta_c)^{2.7}.$$

In [16], the modeling of ceramic sintering based on the described variants of the model was carried out using the finite element method in the COMSOL Multiphysics software. A good agreement between the simulation results and the experimental data was shown.

## 2. SIMULATION RESULTS

The described model of viscous sintering was solved numerically in the three-dimensional case by the finite element method using the FreeFem++ freeware. For the most optimal results of predicting the behavior of the material during sintering, the model parameters must be corrected on the basis of experimental data.

### 2.1. Experimental Data

Samples of sintered ceramic products for experimental confirmation of the results obtained in the course of numerical calculations were made using an additive technological procedure. Samples were prepared from KP-Al<sub>2</sub>O<sub>3</sub>/01 ceramic paste (OOO VunderTekh, Moscow, Russia) based on  $\alpha$ -phase aluminum oxide powder. The average particle size in the powder is  $r = 0.496 \times 10^{-6}$  m. The paste was used as a starting material for 3D printing of 40 parallelepiped-shaped samples,  $45 \times 4 \times 3$  mm in size, in accordance with ASTM C1161 [21]. Samples were printed on a Ceramaker 900 ceramic 3D printer (3DCeram, Maison Rouge, France). After 3D printing, the samples were cleaned from nonpolymerized paste and subjected to primary annealing of the organic binder in a Kittec CLL15 furnace (manufactured by Kittec, Rosenheim, Germany). Annealing was carried out until complete removal of the binder at temperatures below 800 °C. At the final stage of annealing, the samples were heated to a temperature of 1000 °C and kept for one hour; this corresponds to the requirements of the heat treatment procedure recommended by the manufacturer. At the end of the annealing procedure, the samples were naturally cooled in the furnace. The geometric shape and dimensions of the samples after annealing corresponded to the original green body. The annealed samples were divided into eight groups, five samples per group. Seven groups of samples were subjected to high-temperature sintering at temperatures 1100 °C, 1200 °C, 1300 °C, 1400 °C, 1500 °C, 1600 °C, and 1700 °C. Sintering was carried out in the Kittec CLL15 furnace at temperatures 1100–1300 °C due to the limitation on the maximum temperature of this furnace. Sintering at temperatures of 1400–1700 °C was carried out in a ThermConcept HTL 20/17 furnace (ThermConcept, Bremen, Germany). The eighth group of samples was not subjected to sintering. For all forty samples, before and after heat treatment, the geometric dimensions (length, width, height) were measured with a caliper, and the mass was measured using laboratory scales. The effective density of the samples was calculated, and using the known value of the ideal density of  $\alpha$ -phase aluminum oxide, equal to 3.99 g/cm<sup>3</sup>, the residual porosity of the material  $\theta_{\text{exp}}$  was calculated. The results of the average values of porosity and standard deviation  $s$  calculated for each group are presented in Table 1.

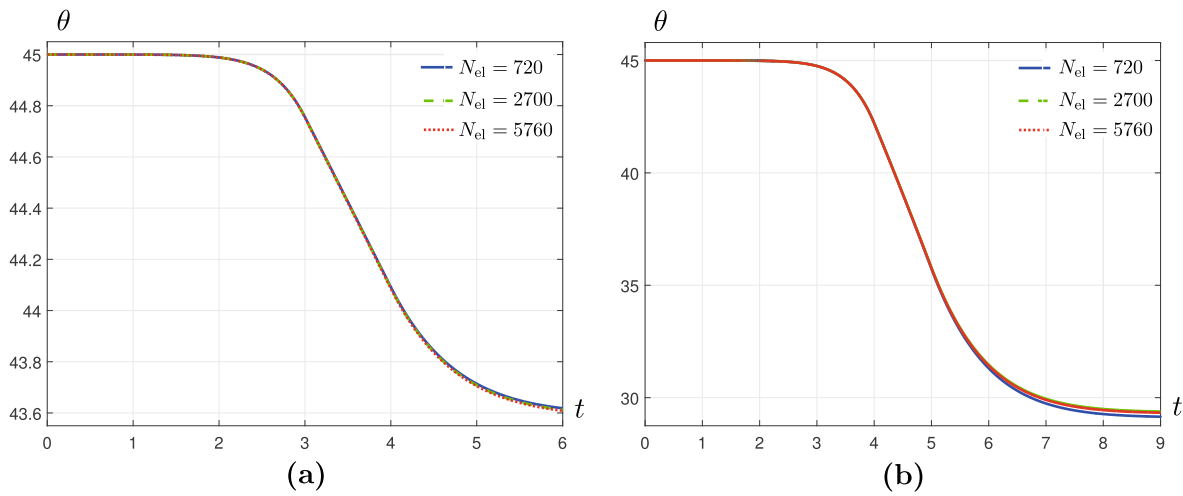


**Fig. 2.** Change in sample porosity during sintering obtained on different computational grids at  $T = 1400^\circ\text{C}$  (a) and  $T = 1600^\circ\text{C}$  (b).

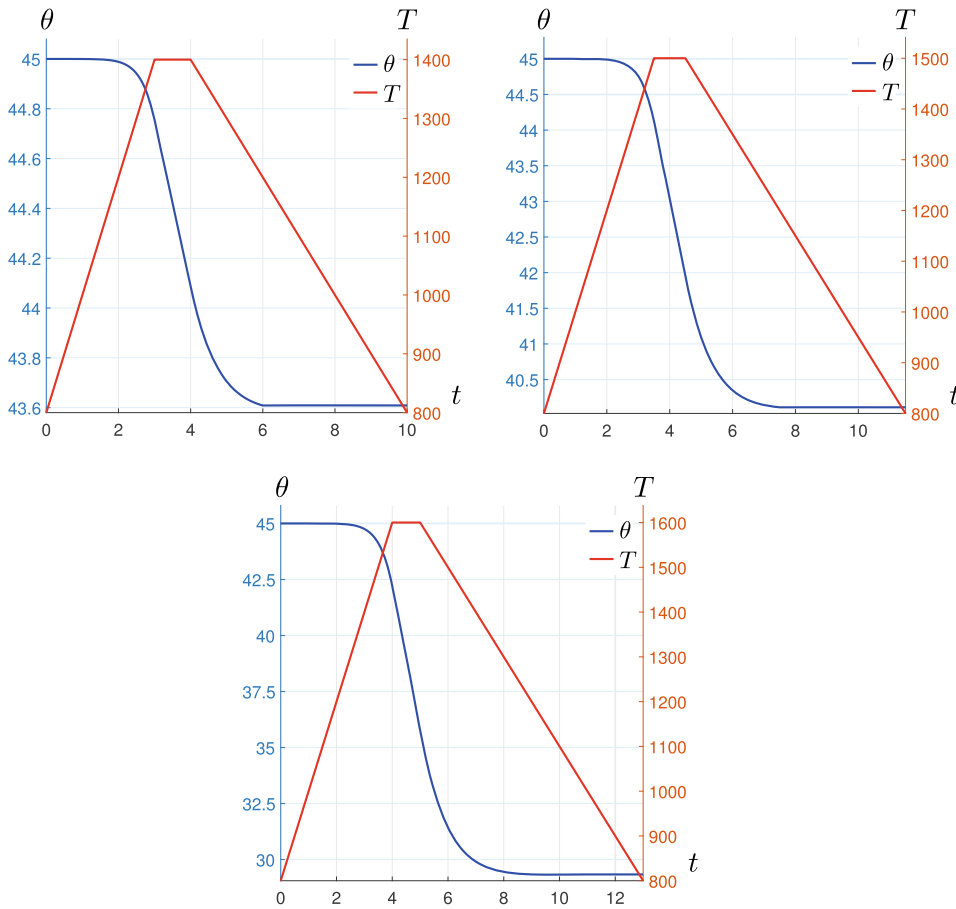


**Fig. 3.** Results of the calculation of the change in sample porosity during sintering.

2.2. Numerical Results

The results of numerical studies are shown in Figs. 2–4.

Since in the considered experimental case, the changes along all axes occur approximately the same way, the main attention in this paper is paid to comparing the change in the porosity of

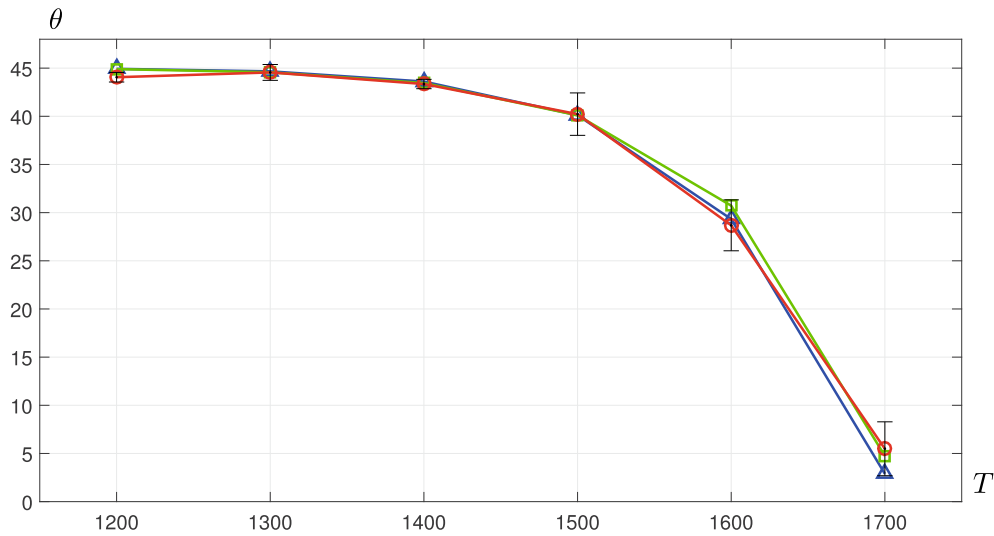


**Fig. 4.** Comparison of experimental and calculated values of sintered sample porosity: (○) experiment, (△) calculations using formula (8), (□) calculations using formula (6).

the material. Calculations were carried out for samples in the form of a parallelepiped with the initial parameters corresponding to those chosen in the experiments. In the framework of this work, two relations were considered for changing the shear viscosity of the material: relation (6) with the following values of constants selected for a specific material:  $A = 1.5 \cdot 10^{-2}$ ,  $B = 33300$ , and  $n = 1$  and relation (8) for  $\eta_{0z} = \eta_{0r}$ . When calculating the sintering stress (4), the value of the surface energy coefficient for  $\text{Al}_2\text{O}_3$  was  $\gamma = 0.9$  [22] and the average particle size in the powder was  $r = 0.496 \times 10^{-6}$  m. Calculations were carried out for three stages of heating: heating at a rate of  $200^\circ\text{C}$  per hour from the initial temperature of  $800^\circ\text{C}$  to  $1200^\circ\text{C}$ ,  $1300^\circ\text{C}$ ,  $1400^\circ\text{C}$ ,  $1500^\circ\text{C}$ ,  $1600^\circ\text{C}$ , and  $1700^\circ\text{C}$ , further exposure for an hour, and cooling at a rate of  $100^\circ\text{C}$  per hour to the temperature of  $800^\circ\text{C}$ . In accordance with experimental data, the initial value of porosity was chosen to be  $\theta = 45\%$ .

In the model configuration, where the calculation of the change in viscosity is performed according to formula (8), the relationship (5) of the change in the modulus of bulk viscosity was corrected taking into account the threshold porosity  $\theta_c = 0.02$  based on the approach proposed in [16],

$$\psi = \frac{2(1-\theta)^3}{3(\theta-\theta_c)}. \quad (9)$$

Figure 2 shows the graphs of porosity change during heating up to  $1600^\circ\text{C}$  calculated on three different grid variants with  $N_{\text{el}} = 720$ ,  $N_{\text{el}} = 2700$ , and  $N_{\text{el}} = 5760$  finite elements using relation (8). Good mesh convergence is observed. In carrying out further calculations, a grid with the number of elements  $N_{\text{el}} = 5760$  was used. The time step was chosen equal to  $ht = 0.01$  s, a value that satisfies the Courant condition.

The results of calculations of the change in porosity with time for three-stage regimes of heating up to temperatures of  $1400^\circ\text{C}$ ,  $1500^\circ\text{C}$ , and  $1600^\circ\text{C}$  are shown in Fig. 3. It can be seen that the curves of changes in  $\theta$  for various heating temperatures have a similar character.

As part of this work, the results of calculating the porosity of the sample were compared with the obtained experimental data. Figure 4 shows two sets of numerical data obtained using different relations for the change in viscosity, (6) and (8). The greatest discrepancy in porosity values is observed at the maximum sintering temperature with the model in (8). In general, a good agreement of the results is shown; this confirms the correctness of the chosen model for describing the change in porosity during sintering of samples from ceramic paste based on aluminum oxide powder.

## CONCLUSIONS

For the development of the ceramic 3D printing industry, it is necessary to be able to qualitatively predict and control the final shape of the product after sintering. In the framework of this paper, we consider a model of viscous sintering whose numerical solution is implemented by the finite element method in the three-dimensional case. The model has been tested by comparison with experimental data on the sintering of samples from alumina ceramic powder fabricated by laser stereolithography. Two options for calculating the change in shear viscosity are considered, material constants are selected for the material under consideration, and good agreement is shown between the results for the porosity of the sintered sample. Thus, the considered model can be chosen as a basis for further development of a more comprehensive approach to modeling the sintering process, including taking into account anisotropy and the possibility of predicting changes in complex product shapes.

## FUNDING

The work was carried out within the framework of a grant from the Republic of Bashkortostan for state support of scientific research conducted under the guidance of leading scientists.

## REFERENCES

1. I. Gibson, D. Rosen, B. Stucker, and M. Khorasani, *Additive Manufacturing Technologies* (Springer Nature, Heidelberg, 2021). <https://doi.org/10.1007/978-3-030-56127-7>
2. Z. Chen, Z. Li, J. Li, Ch. Liu, Ch. Lao, Y. Fu, Ch. Liu, Li Yang, P. Wang, and Y. He, “3D printing of ceramics: A review,” *J. Eur. Ceram. Soc.* **39**, 661–687 (2019). <https://doi.org/10.1016/j.jeurceramsoc.2018.11.013>
3. M. N. Rahaman, *Sintering of Ceramics* (Taylor and Francis, Boca Raton, 2008). <https://doi.org/10.1201/b15869>
4. J. Jhabvala, E. Boillat, and R. Glardon, “Study of the inter-particle necks in selective laser sintering,” *Rapid Prototyping J.* **19** (20), 111–117 (2013). <https://doi.org/10.1108/13552541311302969>
5. H. H. Kart, G. Wang, I. Karaman, and T. Cagin, “Molecular dynamics study of the coalescence of equal and unequal sized Cu nanoparticles,” *Int. J. Modern Phys. C* **20** (02), 179–196 (2009). <https://doi.org/10.1142/S0129183109013534>
6. R. Singh and V. Sharma, “Nano tungsten carbide interactions and mechanical behaviour during sintering: A molecular dynamics study,” *Comput. Mater. Sci.* **197**, 110653 (2021). <https://doi.org/10.1016/j.commatsci.2021.110653>
7. A. Liang, C. Liu, and P. S. Branicio, “Hot-press sintering of aluminum nitride nanoceramics,” *Phys. Rev. Mater.* **5**, 096001 (2021). <https://doi.org/10.1103/PhysRevMaterials.5.096001>
8. S. Nosewicz, J. Rojek, K. Pietrzak, and M. Chmielewski, “Viscoelastic discrete element model of powder sintering,” *Powder Technol.* **246**, 157–168 (2013). <https://doi.org/10.1016/j.powtec.2013.05.020>
9. F. B. Sweidan and H. J. Ryu, “Kinetic Monte Carlo simulations of the sintering microstructural evolution in density graded stainless steel fabricated by SPS,” *Mater. Today Commun.* **26**, 101863 (2021). <https://doi.org/10.1016/j.mtcomm.2020.101863>
10. Y. Liu, M. Militzer, and M. Perez, “Phase field modelling of abnormal grain growth,” *Materials* **12**, 4048 (2019). <https://doi.org/10.3390/ma12244048>
11. G. A. L. van de Vorst, R. M. M. Mattheij, and H. K. Kuiken, “A boundary element solution for two-dimensional viscous sintering,” *J. Comput. Phys.* **100**, 50–63 (1992). [https://doi.org/10.1016/0021-9991\(92\)90309-M](https://doi.org/10.1016/0021-9991(92)90309-M)
12. V. V. Skorohod, *Rheological Basis of the Theory of Sintering* (Naukova Dumka, Kiev, 1972) [in Russian]. <https://doi.org/10.1111/j.1151-2916.1998.tb02768.x>
13. A. van der Laan, R. Epherre, G. Chevallier, Y. Beynet, A. Weibel, and C. Estourn, “Fully coupled electrothermal and mechanical simulation of the production of complex shapes by spark plasma sintering,” *J. Eur. Ceram. Soc.* **41** (7), 4252–4263 (2021). <https://doi.org/10.1016/j.jeurceramsoc.2021.02.010>

14. E. A. Olevsky, "Theory of sintering: From discrete to continuum," *Mater. Sci. Eng.: R: Rep.* **23**, 41–100 (1998). [https://doi.org/10.1016/S0927-796X\(98\)00009-6](https://doi.org/10.1016/S0927-796X(98)00009-6)
15. E. A. Olevsky, S. Kandukuri, and L. Froyen, "Consolidation enhancement in spark-plasma sintering: Impact of high heating rates," *J. Appl. Phys.* **102**, 114913 (2007). <https://doi.org/10.1063/1.2822189>
16. C. Maniere, C. Harnois, and S. Marinel, "3D printing of porcelain and finite element simulation of sintering affected by final stage pore gas pressure," *Mater. Today Commun.* **26**, 102063 (2021). <https://doi.org/10.1016/j.mtcomm.2021.102063>
17. R. M. German, *Sintering theory and practice* (Wiley, Chichester, 1996).
18. A. Safronov, S. Chugunov, A. Tikhonov, M. Gusev, and I. Akhatov, "Numerical simulation of sintering for 3D-printed ceramics via SOVS model," *Ceram. Int.* **45**, 19027–19035 (2019). <https://doi.org/10.1016/j.ceramint.2019.06.144>
19. P. M. Raj and W. R. Cannon, "Anisotropic shrinkage in tape-cast alumina: Role of processing parameters and particle shape," *J. Am. Ceram. Soc.* **82**, 2619 (1999). <https://doi.org/10.1111/j.1151-2916.1999.tb02132.x>
20. E. A. Olevsky, B. Kushnarev, A. Maximenko, V. Tikare, and M. Braginsky, "Modelling of anisotropic sintering in crystalline ceramics," *Philos. J.* **85** (9), 2123–2146 (2005). <https://doi.org/10.1080/14786430412331331989>
21. ASTM Standard C1161-18. *Standard Test Method for Flexural Strength of Advanced Ceramics at Ambient Temperature* (ASTM Int., 2018). <http://www.astm.org>. <https://doi.org/10.1520/C1161-18>
22. N. C. Van, S. K. Sistla, K. S. Van, N. A. Giang, A. Bezold, C. Broeckmann, and F. Lange, "A comparative study of different sintering models for  $\text{Al}_2\text{O}_3$ ," *J. Ceram. Soc. Jpn.* **124**, 301–312 (2016). <https://doi.org/10.2109/jcersj2.15257>